doi:10.1017/S1431927622003002
Microsc. Microanal. 28 (Suppl 1), 2022

Quantitative EPMA and Compositional Mapping of Nakhlite Northwest Africa 14369

P. K. Carpenter[1], A.J. Irving[2], C.J.-K Yen[1] and B.L. Jolliff[1]

[1.] Dept. of Earth and Planetary Sciences and McDonnell Center for the Space Sciences, Washington University, Saint Louis, MO, USA.
[2.] Dept. of Earth & Space Sciences, University of Washington, Seattle, WA, USA.

Meteorites represent important samples of planetary materials, and electron-probe microanalysis (EPMA) is fundamental to their characterization, classification, and petrologic interpretation. Large-scale backscattered-electron (BSE) and X-ray stage maps are used for location of analytical areas of interest. We continue development of quantitative compositional mapping using wavelength-dispersive spectrometry with full matrix correction at each pixel. These data sets are used for elemental and mineral stoichiometric analysis, calculation of area fraction, and modal recombination analysis. Important microanalysis issues include pixel size sampling and recognition of multiphase pixels, and background correction and detection limit considerations. These methods have been applied to martian nakhlites Northwest Africa (NWA) 13368 [1] and for this study NWA 14369 [2]. Nakhlites are cumulate igneous rocks with early-crystallized olivine followed by crystallization of zoned Ca-pyroxene (pigeonite and augite), with interstitial feldspathic glass and/or plagioclase [3]. Fig. 1 shows Al-Mg-Fe RGB X-ray intensity maps acquired on a polished thin section containing two sequential butterfly slices of NWA 14369. In these maps olivine is blue-green, augite is green, and interstitial plagioclase is red. Area proportions for the left and right fragments were measured using ImageJ binary image processing.

With quantitative EPMA compositional mapping, a complete analysis is obtained at each pixel, for a 1024x1024 stage map there are $1024^{\wedge 2}$ analyses, a number of which fall on cracks and pits and others which sample multiple phases at mineral grain boundaries. Analytical totals at each pixel are used to screen these from further processing. We present here results using cation stoichiometry analysis for assessment of accuracy and for use in mineral classification and phase discrimination. For quantitative compositional analysis of meteorites, classification relies on olivine, pyroxene, and plagioclase. The analytical results include mineral formula calculation on a 24 oxygen basis. This allows processing of olivine with simplified nominal formula of A_2SiO_4 as $A_{12}Si_6O_{24}$ with A=Mg,Fe, and similarly for pyroxene $A_xB_{2-x}Si_2O_6$ as $A_{4x}B_{8-4x}Si_8O_{24}$ (with A=Mg,Fe and B=Ca with x range 0-2), and feldspar $A_{1-x}B_xAl_{1+x}Si_{3-x}O_8$ as $A_{3-3x}B_{3x}Al_{3+3x}Si_{9-3x}O_{24}$ (with A=Na,K and B=Ca with x range 0 to 1). The cation sums for these phases, originally 3, 4, and 5, are 18, 16, and 15, respectively. These relations are also used to calculate the mineral end-members for olivine (Fo,Fa), pyroxene (Wo,En,Fs), and feldspar (Ab,Or,An).

A quantitative map was acquired on a zoned olivine from the left-side fragment of nakhlite 14369 in Fig. 1. The resulting analytical data include elemental, oxide, and cation stoichiometric values, and a representative map is shown in Fig. 1C for MgO oxide wt. percent. Because the olivine shows Mg-Fe rim zoning with concentration values similar to the augite, it is not straightforward to classify olivine vs. pyroxene without using cluster analysis. Fig. 2B is a histogram of cation sum data for the map area which shows distinct peaks for olivine (18), pyroxene (16), and plagioclase (15). The normal distribution of these peaks emphasizes the sampling nature which includes counting statistics and variable accuracy due to phase boundaries and surface features. Fig. 2A shows a classification map based on selection of pixels with the cation sum values for olivine, pyroxene, and plagioclase, and demonstrates the powerful con-

straint that stoichiometry places on phase identification. For the pixels which satisfy the stoichiometric constraint for olivine, further processing to calculate olivine forsterite and fayalite molecular percent results in the histogram in Fig. 2C which shows a peak for Fa_{62} and a step distribution extending to Fa_{82}. These values agree with spot analyses of the homogeneous olivine core and the progressive change in composition of the olivine rim. Finally, Fig. 2D shows map data for olivine fayalite content, and is contoured with a color scheme to highlight the range $Fa_{62\text{-}82}$. Using data extracted from this map, a profile of olivine fayalite content vs. distance is shown as an inset for an arbitrary scan indicated by the blue line.

This example illustrates the powerful constraints by sequential screening of the analytical total, cation sum, and further processing to perform calculations previously restricted to conventional spot analyses.

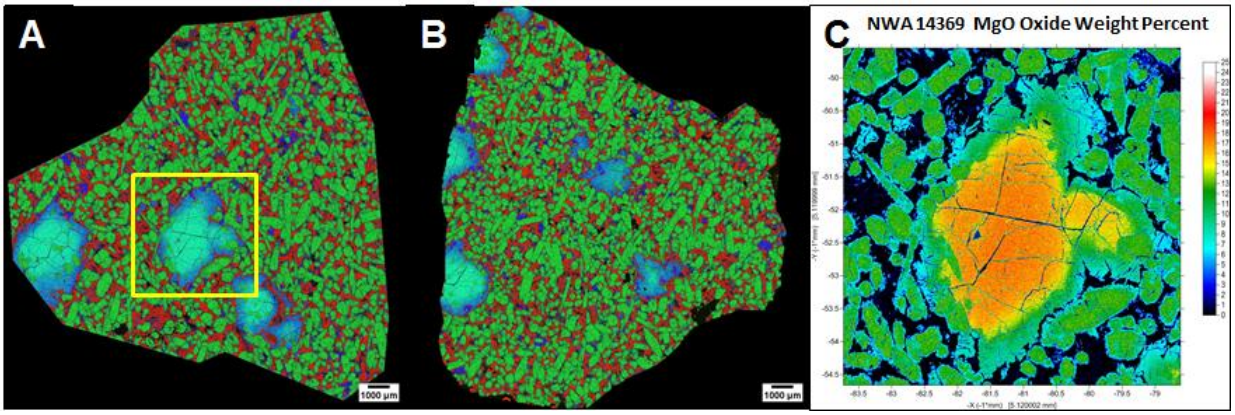

Figure 1. Nakhlite NWA 14369. **A and B.** Al-Mg-Fe RGB composite X-ray maps. Olivine is blue with Mg-Fe zoning, augite is green with similar zoning, and interstitial plagioclase is red. Modal proportions in area percent: LHS fragment: olivine 23.3, augite 54.9, interstitial plagioclase 21.8; RHS fragment: olivine 18.1, augite. 61.1, and plagioclase 20.7. **C.** Quantitative map of area outlined in Fig. 1A with contoured data for MgO oxide weight percent.

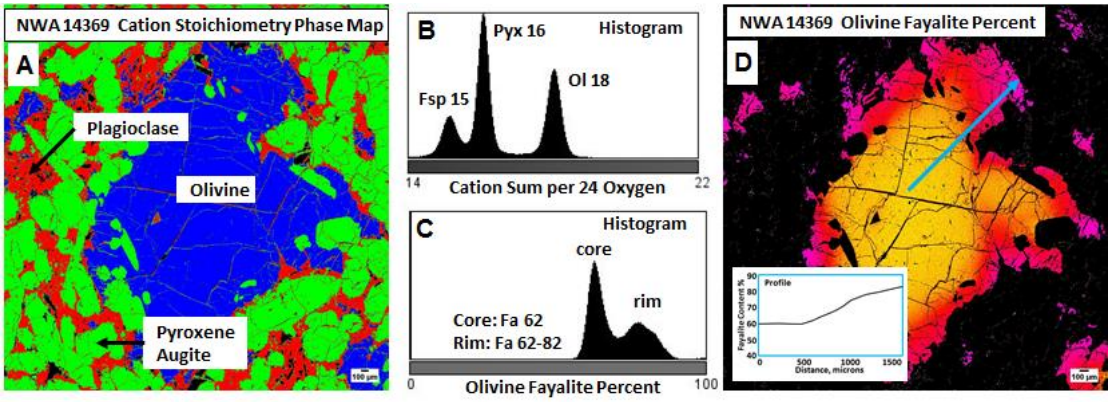

Figure 2. A. Phase classification based solely on mineral cation sum using histogram data in. **B**. **Figure 2 C.** Calculated olivine fayalite composition for all pixels classified as olivine with histogram showing homogeneous core and progressively zoned rim. **D.** Resulting phase map for olivine with color scale for fayalite content 62-82 percent and inset line profile for core-rim traverse extracted from map data set.

https://doi.org/10.1017/S1431927622003002 Published online by Cambridge University Press

References:

[1] PK Carpenter et. al., 52nd LPSC. (2020).
[2] PK Carpenter et. al., 53rd LPSC. (2022).
[3] A Treiman, Chemie Erde **65** (2005), p. 203.

https://doi.org/10.1017/S1431927622003002 Published online by Cambridge University Press